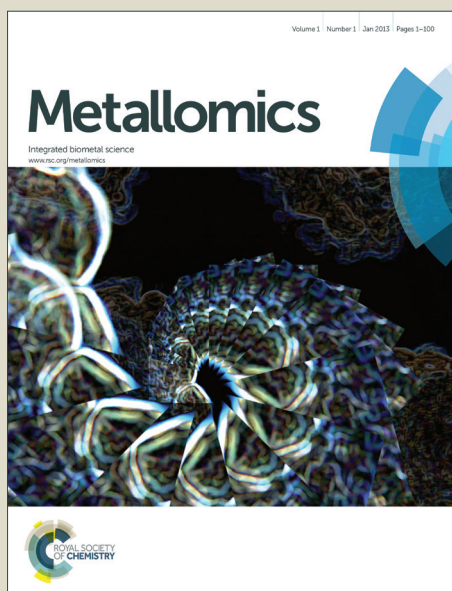


Metallomics

Accepted Manuscript



This is an *Accepted Manuscript*, which has been through the Royal Society of Chemistry peer review process and has been accepted for publication.

Accepted Manuscripts are published online shortly after acceptance, before technical editing, formatting and proof reading. Using this free service, authors can make their results available to the community, in citable form, before we publish the edited article. We will replace this *Accepted Manuscript* with the edited and formatted *Advance Article* as soon as it is available.

You can find more information about *Accepted Manuscripts* in the [Information for Authors](#).

Please note that technical editing may introduce minor changes to the text and/or graphics, which may alter content. The journal's standard [Terms & Conditions](#) and the [Ethical guidelines](#) still apply. In no event shall the Royal Society of Chemistry be held responsible for any errors or omissions in this *Accepted Manuscript* or any consequences arising from the use of any information it contains.

1
2
3
4
5
6
7
8
9
10
11
12
13
14
15
16
17
18
19
20
21
22
23
24
25
26
27
28
29
30
31
32
33
34
35
36
37
38
39
40
41
42
43
44
45
46
47
48
49
50
51
52
53
54
55
56
57
58
59
60

1
2
3
4
5
6
7
8
9
10
11
12
13
14
15
16
17
18
19
20
21
22
23
24
25
26
27
28
29
30
31
32
33
34
35
36
37
38
39
40
41
42
43
44
45
46
47
48
49
50

Deregulation of biometal homeostasis: the missing link for neuronal ceroid lipofuscinoses?

Alexandra Grubman,^a Eveliina Pollari,^b Clare Duncan,^a Aphrodite Caragounis,^a Tea Blom,^c Irene Volitakis,^d Andrew Wong,^e Jonathan Cooper,^e Peter J. Crouch,^a Jari Koistinaho,^b Anu Jalanko,^c Anthony R. White,^a Katja M. Kanninen.^b

^aDepartment of Pathology, The University of Melbourne, Victoria, Australia.

^bA.I. Virtanen Institute for Molecular Sciences, University of Eastern Finland, Kuopio, Finland.

^cNational Institute for Health and Welfare, Public Health Genomics Unit, Helsinki, Finland.

^dFlorey Institute of Neuroscience and Mental Health, The University of Melbourne, Victoria, Australia.

^eDepartment of Neuroscience, King's College, London, UK.

TABLE OF CONTENTS ENTRY

Deregulation of biologically active metal homeostasis is a feature of 4 genetically distinct variants of neuronal ceroid lipofuscinoses, a group of fatal neurodegenerative disorders.

ABSTRACT

Neuronal ceroid lipofuscinoses (NCLs), a group of genetically distinct fatal neurodegenerative disorders with no treatment or cure, are clinically characterised by progressive motor and visual decline leading to premature death. While the underlying pathological mechanisms are yet to be precisely determined, the diseases share several common features including inflammation, lysosomal lipofuscin deposits and lipid abnormalities. An important hallmark of most common neurodegenerative disorders including Alzheimer's, Parkinson's and motor neuron diseases is deregulation of biologically active metal homeostasis. Metals such as zinc, copper and iron are critical enzyme cofactors and are important for synaptic transmission in the brain, but can mediate oxidative neurotoxicity when homeostatic regulatory mechanisms fail. We previously demonstrated biometal accumulation and altered biometal transporter expression in 3 animal models of CLN6 NCL disease. In this study we investigated the hypothesis that altered biometal homeostasis may be a feature of NCLs in general using 3 additional animal models of CLN1, CLN3 and CLN5 disease. We demonstrated significant accumulation of the biometals zinc, copper, manganese, iron and cobalt in these mice. Patterns of biometal accumulation in each model preceded significant neurodegeneration, and paralleled the relative severity of disease previously described for each model. Additionally, we observed deregulation of transcripts encoding the anti-oxidant protein, metallothionein (Mt), indicative of disruptions to biometal homeostasis. These results demonstrate that altered biometal homeostasis is a key feature of at least 4 genetically distinct forms of NCL disease.

INTRODUCTION

NCLs are a group of inherited fatal lysosomal storage disorders (LSDs) with neurological involvement. There are currently 14 recognized forms of NCLs that are distinguished by genetic deficit (CLN1-14) and different ages of onset ranging from congenital to adult, although most variants manifest during childhood. Symptoms also vary in severity and rate of progression, but commonly include epileptic seizures, progressive dementia, blindness and motor decline leading to paralysis and premature death (reviewed in ¹).

The development of mouse models that closely recapitulate relevant disease features has been instrumental to investigation of disease mechanisms, and assessment of treatment efficacy. Infantile NCL (INCL) is caused by mutations in the gene encoding palmitoyl protein thioesterase 1, PPT1/CLN1, a lysosomal enzyme involved in depalmitoylation of S-acylated proteins.² The severe nature and early onset of CLN1 disease is replicated in *Cln1* knockout (ko) mice lacking exon 4,³ that show early loss of vision by 3.5 months, clapping and seizures by 4 months and myoclonic jerks by 6 months of age. The progression of the disease results in a hind limb paralysis at the average age of 5.2 months, followed by death at approximately 6.5 months. The brain mass of *Cln1* ko mice is remarkably reduced due to cortical atrophy. Storage material, a prominent pathological feature in NCL patients,¹ is abundant in the brain at the age of 3 months, and continues to accumulate in the brain and retina until the age of 6 months. Another *Cln1* ko mouse model containing a neomycin resistance gene inserted instead of exon 9, lacks an obvious progressive visual impairment phenotype, although myoclonic jerks and clapping behaviors are similar to those observed in the exon 4 ko animals.⁴

By contrast, the most common NCL variant, called Juvenile NCL (JNCL) or Batten disease is a milder form of disease. JNCL is caused by defects in *CLN3*, which encodes a putative transporter localized to multiple cellular compartments, postulated to be involved in regulation of intracellular pH and osmotic shock responses.^{5,6} A number of knock in and ko mice modeling CLN3 disease have been generated. The most widely used to date are *Cln3ΔEx7-8* and *Cln3ΔEx1-6* ko mice.^{7,8} Similar to disease progression in patients, these murine models exhibit milder symptoms and later onset compared to the *Cln1* mice. Storage material is evident prior to birth in *Cln3ΔEx7-8* mice, expressing the most common human *CLN3* mutation, a ~1kb deletion.⁷ The mice display gait abnormalities, clapping behavior, reduced retinal photoreceptor numbers and an 80% survival rate by 12 months of age.⁷ *Cln3ΔEx1-6* mice are largely asymptomatic until 12 months, although autofluorescent cortical inclusions and decreased cortical volume due to loss of parvalbumin-positive interneurons are evident from 5 and 7 months of age, respectively.⁸ Moreover, a later study reported that *Cln3ΔEx1-6* mice displayed impaired motor function from post-natal day 14, and significant inflammatory phenotypes including activated cerebellar Bergmann glia.⁹

Variant late infantile NCL (vLINCL) is caused by mutations in *CLN5*, encoding a lysosomal glycoprotein¹⁰ of unknown function with a putative role in ceramide synthesis.¹¹ vLINCL is milder than CLN1, but more aggressive than CLN3 disease. Similarly, the mouse model for CLN5 disease, which encodes a truncated protein due

1 to the deletion of exon 3,¹² displays an intermediate phenotype compared to *Cln1* and
2 *Cln3* ko animals. *Cln5* ko mice lose vision at the age of 5.2 months, but show no
3 motor dysfunction or brain atrophy.¹² The presence of storage material, with a
4 characteristic vLINCL fingerprint and curvilinear profile begins at the age of 3
5 months, and accumulation of autofluorescence throughout the brain is evident by 6
6 months.

7
8 These mouse models, as well as others, with genetic defects in CLN2/TPP1, CLN6,
9 CLN8, CLN10/Cathepsin D (reviewed in ¹³), have yielded an immense amount of
10 biochemical and mechanistic information on the similarities and differences between
11 different forms of NCLs. It is now established that the NCL gene products are
12 localized throughout the cell: in the lysosome (CLN1/PPT1, CLN2/TPP1, CLN5,
13 CLN10/Cathepsin D, CLN13/Cathepsin F CLN12/ATP13a2, CLN7), the endoplasmic
14 reticulum (CLN6, CLN8), the secretory pathway (CLN3, CLN4), the cytoplasm
15 (CLN14/KCTD7) or are extracellular (CLN11/progranulin; reviewed in ¹⁴). In
16 contrast to most other LSDs, only 4 of the NCL-causative genes encode lysosomal
17 enzymes (CLN1/PPT1, CLN2/TPP1, CLN10/Cathepsin D, CLN13/Cathepsin F). The
18 functions of the majority of the NCL proteins remain unknown, although
19 CLN12/ATP13a2 and CLN14/KCTD6 are postulated to act as ion channels. Unlike
20 most classical LSDs, lysosomal storage of lipofuscin material in NCLs is not directly
21 associated with defective lysosomal enzymes that prevent degradation of particular
22 substrates, and is also not predictive of regional neuronal pathology.¹⁵ Another
23 common pathological feature for this group of genetically distinct but clinically
24 related disorders is inflammation;^{3, 12} activated brain astrocytes and glia are evident
25 prior to birth in some NCL models and spatially parallel subsequent neuronal
26 pathology.¹⁵ Impaired cellular lipid metabolism has also been implicated in several
27 NCL forms; reports in both patients and mouse NCL models indicate the presence of
28 altered serum lipid profiles,¹⁶ elevated cholesterol^{17, 18} and aberrant storage of
29 phospholipids.¹⁹ Moreover, CLN1/PPT1 and CLN3 have been detected in lipid
30 rafts,^{20, 21} consistent with a role in maintenance of cellular lipid dynamics. Interactions
31 between several subsets of NCL proteins, including those between CLN5 and
32 CLN1/PPT1, CLN2/TPP1, CLN3, CLN6 or CLN8,²² are indicative of common
33 pathogenic mechanisms, but these are yet to be precisely delineated. This is further
34 confounded by the cell-specific physiological central nervous system (CNS)
35 expression levels of each NCL protein – CLN1 is primarily expressed in neurons and
36 astrocytes, while CLN3 levels are greatest in neurons and microglia,²³ and microglia
37 express a high amount of CLN5.¹⁸ Hence, while it appears that convergent molecular
38 processes may account for some pathological NCL traits, the current understanding of
39 the mechanisms involved is limited.

40
41 A common hallmark of neurodegeneration is the deregulation of biologically active
42 metal homeostasis.²⁴ Tight cellular control over metals such as zinc, copper and iron
43 is critical – these metals comprise enzyme cofactors of over 10% of all proteins,²⁵ but
44 can induce toxic oxidative damage if concentrations of labile metal pools rise.²⁶ The
45 particular vulnerability of the brain to metal dyshomeostasis is supported by the vast
46 number of neurodegenerative diseases with metal handling abnormalities, including
47 Alzheimer's, Parkinson's and motor neuron diseases, and the demonstrated
48 therapeutic efficacy of metal-targeted treatments.²⁷⁻³⁰ We have previously shown that
49 changes to biometal homeostasis also drive pathology in 3 natural models of CLN6
50 NCL,^{31, 32} involving aberrant expression of the ER/Golgi resident biometal

1 transporter, *Zip7* (manuscript submitted). Moreover, we reported that biometal
2 accumulation in CLN6 tissues involved dramatic compensatory upregulation of the
3 metal sequestering protein, Mt.³² Here, using an additional 3 genetically distinct NCL
4 mouse models, we demonstrate that the aberrant metal accumulation and Mt
5 overexpression phenotype is common to multiple forms of NCLs, including CLN1,
6 CLN3 and CLN5 variants. Aside from inflammation, lipid metabolism and lipofuscin
7 accumulation, alterations to metal homeostasis appear to represent an additional
8 phenotypic characteristic common to multiple forms of NCLs, including variants
9 caused by both soluble and membrane bound gene products that are present in
10 different cellular compartments.

11 RESULTS

12 Biomaterials accumulate in the brains of NCL model mice

13 We previously showed that aberrant biometal accumulation contributes to disease
14 pathology in 3 natural animal models of CLN6 disease. To determine whether
15 impaired biometal homeostasis is a pathological feature common to multiple forms of
16 NCLs, we investigated the metal content in CNS tissues of mice modeling CLN1,
17 CLN3 and CLN5 diseases. At least one presymptomatic and one post-symptom onset
18 age was chosen to perform analyses for each model. *Cln1* ko mice are phenotypically
19 normal until 3.5 months of age, when visual dysfunction first becomes apparent
20 (Table 1). The lifespan of these mice is approximately 6.5 months. *Cln5* ko mice
21 develop vision loss after 5 months of age, but do not exhibit motor deficits. *Cln3* ko
22 mice display symptoms after 12 months, but some neuronal loss is evident by 7
23 months. We therefore chose the following ages for analysis: for *Cln1* ko mice- 3,4, and
24 5 months; for *Cln5* ko mice – 3,4,5 and 7 months; and for *Cln3* ko mice- 6 and 12
25 months. We examined the following CNS tissue regions in *Cln1* and *Cln5* ko mice:
26 olfactory bulb, cortex, cerebellum, hippocampus and spinal cord. In *Cln3* ko mice, we
27 analysed the brainstem, cortex, thalamus, and spinal cord. The thalamus was included
28 for *Cln3* ko mice, as this was previously reported to be an important region for
29 pathology in this model at 12 months of age.⁵ Due to limited material, not all analyses
30 could be performed on all animals and all ages. The levels of zinc, copper,
31 manganese, cobalt and iron were significantly elevated in NCL model mice. Due to
32 the complexity of the current study, we focused only on the changes observed to
33 metals that are primarily protein-bound in biological tissues. Therefore, the
34 examination of changes to additional, biologically important free metals, including
35 calcium, magnesium, potassium and sodium is outside the scope of this study and will
36 be reported elsewhere.

37 A significant increase in zinc concentrations was detected in the olfactory bulb in 3
38 month-old *Cln1* ko mice (Fig. 1A), progressing to the cortex and cerebellum by 4
39 months of age (Fig. 1B). By 5 months of age, significantly elevated zinc was detected
40 in all brain regions analysed in these mice, the most dramatic in the olfactory bulb
41 with a 90% increase above the levels in wild-type mice (Fig. 1C). As these mice
42 succumb to disease at ~6.5 months, no further tissue sampling was performed after 5
43 months. *Cln5* ko mice, which develop a milder form of disease, displayed a trend of
44 increased metal content in all CNS regions by 5 months of age, which reached
45 statistical significance by 7 months of age (Fig. 1D). Zinc concentrations were
46 increased by between 34% in the hippocampus to 130% in the olfactory bulb. No
47 significant changes to zinc content were detected in CLN3 mice, although a trend
48
49
50

1
2
3 1 towards increased zinc in the cortex and thalamus of 6 month-old mice was observed
4 2 (Fig. 1E-F).
5 3

6 4 Changes in CNS copper concentrations in *Cln1* and *Cln5* ko mice largely paralleled
7 5 the changes observed for zinc. In *Cln1* ko mice, copper was increased significantly in
8 6 the olfactory bulb at 3 months (Fig. 2A), in the cortex and cerebellum at 4 months
9 7 (Fig. 2B) and within all brain structures tested at 5 months, except the cerebellum,
10 8 where the observed increase did not reach statistical significance (Fig. 2C). The rise in
11 9 copper concentrations was 114% greater than in controls in the olfactory bulb. A trend
12 10 of elevation in copper concentrations was observed in *Cln5* ko mice from 4 months of
13 11 age, with statistically significant rises in copper being evident in the hippocampus in 5
14 12 month-old mice (Fig 2B-C). By 7 months of age, CNS-wide dramatic increases of 80-
15 13 220% in copper concentrations were observed in CLN5 mice (Fig. 2D). In 6 month-
16 14 old *Cln3* ko mice, copper levels were significantly increased in the thalamus, and an
17 15 overall increase was observed in CNS tissues (Fig. 2E). By 12 months of age,
18 16 however, copper levels were not significantly different to those of wild-type mice
19 17 (Fig. 2F).
20 18

21 19 Similarly, manganese concentrations were progressively elevated in *Cln1* and *Cln5* ko
22 20 mice over the course of disease. Analogous to copper and zinc, elevated manganese
23 21 content was first detected in the olfactory bulb of 3 month-old *Cln1* ko mice (Fig.
24 22 3A), then the cortex, cerebellum and spinal cord at 4 months (Fig. 3B) and all regions
25 23 by 5 months, except the hippocampus where the rise did not reach significance (Fig.
26 24 3C). Manganese accumulation was detected in the cortex, olfactory bulb and spinal
27 25 cord in *Cln5* ko mice at 7 months of age (Fig. 3D). However, no changes to
28 26 manganese concentrations were observed in *Cln3* ko animals (Fig. 3E-F).
29 27

30 28 The early alterations to iron levels in *Cln1* ko mice followed the regional pattern
31 29 described for zinc, copper and manganese, however, by 5 months of age, iron was
32 30 only increased in the cerebellum and olfactory bulb (Fig. 4A-C). Similarly, the most
33 31 pronounced iron elevation in *Cln5* ko mice was observed in the olfactory bulb,
34 32 cerebellum and spinal cord at 7 months of age (Fig. 4D). While iron concentrations
35 33 did not differ between WT and *Cln3* ko animals at 6 months (Fig. 4E), at 12 months,
36 34 there was a significant overall increase in iron content in the CNS of *Cln3* ko mice
37 35 (Fig. 4E-F).
38 36

39 37 Striking changes to cobalt concentrations were evident in *Cln1*, *Cln3* and *Cln5* ko
40 38 mice. Similar to the metals described above, cobalt accumulation began in the
41 39 olfactory bulb in 3 month-old *Cln1* ko animals, progressing to the cortex, cerebellum
42 40 and spinal cord by 4 months, and all CNS tissues except for the hippocampus by 5
43 41 months (Fig. 5A-C). Interestingly, cobalt levels were substantially reduced in
44 42 hippocampi of 3 month-old *Cln1* ko mice, the only metal we found to be deficient in
45 43 any tissue tested. Widespread rises in cobalt concentrations in the cerebellum, cortex
46 44 and olfactory bulb at 5 months were the earliest metal changes detected in *Cln5* ko
47 45 mice, and were progressively increased in every tissue except the hippocampus by 7
48 46 months (Fig. 5C-D). Cobalt concentrations were also increased in the CNS of 6
49 47 month-old *Cln3* ko mice, but stabilized by 12 months of age (Fig. 5E-F). Cobalt
50 48 content in the thalamus was below the level of detection in either WT or *Cln3* ko
51 49 animals.
52 50
53
54
55
56
57
58
59
60

1 Our previous reports indicated that the heart and liver were also sites of biometal
2 accumulation in 3 natural CLN6 sheep and mouse models.^{31,32} However, we detected
3 no differences in the concentrations of zinc, copper, manganese, iron or cobalt in the
4 livers or hearts of *Cln1*, *Cln3* or *Cln5* ko mice at any age (Fig. S1-2), suggesting that
5 aberrant biometal homeostasis originates specifically in CNS tissues in these models.
6 Taken together, these data demonstrate dramatic and broadly progressive regional
7 CNS accumulation of biometals throughout the disease course in *Cln1* and *Cln5* ko
8 mice, and more subtle regional changes to copper, iron and cobalt in *Cln3* ko mice,
9 highlighting the complex nature of spatio-temporal biometal disturbances in the brains
10 of animals with NCL diseases.

11 **Elevated Mt expression in NCL model mice**

12 We next examined expression of transcripts encoding various isoforms of the metal
13 sequestering and anti-oxidant acute phase protein, Mt, to verify early disease-
14 associated changes to metal homeostasis in NCL model mice. While it would be
15 advantageous to also measure Mt protein levels, most commercially available
16 antibodies to Mt do not distinguish between Mt isoforms and detect bands ranging
17 from 28-35kDa, whereas the molecular weight of Mt ranges from 5 to 14 kDa.
18 Moreover, there is no evidence of post-transcriptional or post-translational regulation
19 of Mt isoforms in the brain. Therefore quantitative changes to *Mt* transcripts provide
20 an additional indicator of disrupted metal homeostasis. We chose to perform analyses
21 for *Cln1* and *Cln5* ko mice in the cortical region, due to the significant metal changes
22 observed in the cortex (Fig. 1-5), previously demonstrated similarities between
23 cortical transcriptional profiles in *Cln1* and *Cln5* ko mice,³³ and, because the cortex is
24 the initial site of significant neuron loss in *Cln5* ko mice.³⁴ For *Cln3* ko mice, the
25 cerebellum was chosen as it was reported to represent an important region of
26 pathology in these animals⁹ and JNCL patients.³⁵ We also compared *Mt* expression in
27 the *Cln1*, *Cln3* and *Cln5* ko mice with *Cln6 nclf* mice (Table 1). We previously
28 reported changes to metal homeostasis in the cortex and spinal cord in 3 month-old
29 *Cln6 nclf* mice, whereas the cerebellum was a later site of dramatic metal
30 accumulation.³¹ We therefore analysed *Mt* gene expression in cortices, cerebella and
31 spinal cords of *Cln6 nclf* mice.

32
33
34 The *Mt1* and *Mt2* transcripts were significantly upregulated in 5 month-old *Cln1* ko
35 mice, and were also both increased by 1.9 fold in 5 month-old *Cln5* ko mice, although
36 this did not reach statistical significance (Fig. 6A). *Mt3* mRNA was also 2.2 and 1.4
37 fold elevated, respectively, in *Cln1* and *Cln5* ko mice. These data are consistent with
38 increased cortical copper and zinc, both capable of strongly inducing *Mt* transcription.
39 An overall significant increase of *Mt* expression was observed in the cerebella of 6
40 month-old CLN3 mice, although this did not reach statistical significance for any
41 single *Mt* transcript (Fig. 6B). We also compared *Mt* expression in the cortex,
42 cerebellum and spinal cord of 3 month-old pre-symptomatic *Cln6 nclf* mice.
43 Interestingly, while no significant changes to *Mt1* or *Mt3* transcription were detected
44 (Fig. 6C-E), we observed significant deregulation of *Mt2* in the brains of *Cln6 nclf*
45 mice (Fig. 6E, F). In the spinal cord, where we previously reported zinc and
46 manganese accumulation at this age,³¹ *Mt2* was greater than 2 fold overexpressed,
47 whereas in the cerebellum, the site of inflammatory responses at this age (A.
48 Grubman, unpublished observations), *Mt2* expression was dramatically reduced
49 compared to control mice. Aberrant *Mt* expression in multiple models further
50 emphasizes the deregulation of CNS biometal homeostasis in NCL model mice.

Metal transport protein expression in NCL model mice

Aside from cytoplasmic buffering of excess labile metal pools by Mt,³⁶ subcellular metal trafficking dynamics are mediated by membrane-bound metal transport proteins.³⁷ We previously reported that the ER/Golgi-resident zinc influx transporter, Zip7, was aberrantly expressed in two natural CLN6 sheep models (manuscript submitted) and the natural *Cln6 nclf* mouse model.³¹ We also detected changes to other transporters of the Zip/SLC39A and ZnT/SLC30A families that are primarily known to transport zinc, but not to the copper transporters CTR1, CTR2 or ATP7A/B, despite the greater changes to copper in the brains of those animals. We therefore investigated whether changes to biometal transport proteins of the Zip (Zip7, 8,14) and ZnT (ZnT5, 6,7) families also occur in *Cln1*, *Cln3* and *Cln5* ko mice. We detected no changes in expression of any metal transport proteins tested in the cerebella of 5 and 7 month-old *Cln1* or *Cln5* ko mice, respectively (Fig 7). We were unable to detect expression of Zip14, ZnT5 or ZnT7 protein in either 5 month-old WT Rcc or *Cln1* animals. Given that expression is detectable in 7 month-old WT Rcc animals (Fig. 7), it is possible that these proteins are regulated in an age-dependent manner in the brains of the Rcc strain of mice. However, a ~30kDa Zip7-reactive band was specifically upregulated in CLN5 mice. This corresponds to a predicted low molecular weight isoform of Zip7 (Ensembl Havana Protein ID ENSMUSP00000133146) containing a histidine-rich region and a Zip domain.

GAPDH and tubulin expression did not correlate to total protein content in *Cln3* ko mice (data not shown) which may reflect previously reported impaired ATP production in human CLN3 disease³⁸ and cytoskeletal abnormalities in *Cln3* mouse neurons,³⁹ precluding from using these markers as loading controls. Therefore, for *Cln3* ko mice, total ERK was used as a loading control. No significant differences were detected in the expression levels of any of the Zip or ZnT proteins analysed. However, there was a trend towards increased expression of ZnT7 in the *Cln3* ko cerebella. Together, the data demonstrate that biometal accumulation in CNS tissues in *Cln1*, *Cln3*, and *Cln5* ko mice occurs in the absence of significant tissue-level alterations to metal transporter expression.

DISCUSSION

We previously reported accumulation of zinc, copper, iron, manganese and cobalt in the disease-affected occipital lobe in 2 sheep models of CLN6 disease and the mouse *Cln6 nclf* model.^{31, 32} Deregulation of metal homeostasis was associated with early and progressive changes to the ER/Golgi localized metal transporter, Zip7, as well as subsequent changes to other transporters including Zip8, Zip14, ZnT6 and ZnT7 after symptom onset (manuscript submitted). In this study, we sought to determine whether deregulation of biometal homeostasis is a common feature to multiple forms of NCLs. We therefore investigated metal metabolism in 3 additional genetic NCL diseases with different molecular disturbances and different underlying pathogenic mechanisms. Indeed, zinc, copper, iron, manganese and cobalt levels were elevated in *Cln1*, *Cln3* and *Cln5* ko animals, indicating that impaired metal homeostasis is not a CLN6 disease-specific phenotype. Consistent with this, a previous microarray study reported changes in ZnT6 transcripts in *Cln3ΔEx7-8* and *Cln6 nclf* mouse cerebellar neuron precursor cell lines.⁴⁰ Moreover, two of the genes mutated in NCLs are metal

1 transporters: ATP13A2, the cause of an adult onset form of NCL, Kuf's disease,⁴¹⁻⁴³ is
2 a lysosomal cation transporter, and CLN14 is postulated to encode a potassium
3 channel,⁴⁴ demonstrating metal transport abnormalities in two additional NCL
4 variants. Together, these studies and our data demonstrate common molecular defects
5 potentially indicating convergent pathogenic processes in these related but distinct
6 disorders.

7
8 Zinc is critical for synaptic transmission and is bound by over 3000 proteins, while
9 labile zinc levels are kept low by transport and buffering systems to prevent
10 neurotoxicity. Unregulated labile zinc overload in particular organelles can cause cell
11 death via oxidative induction of mitochondrial membrane depolarization or
12 autophagy-mediated lysosomal dysfunction.^{45,46} However, localized zinc deficiencies
13 are also damaging to neuronal function, as ZnT3 ko mice lacking synaptic zinc
14 display cognitive disabilities.⁴⁷ Thus there is a "set point" or optimal labile zinc
15 concentration in each organelle, which can vary from sub-picomolar in the ER and
16 Golgi,⁴⁸ low picomolar in the cytoplasm,⁴⁹ to high micromolar in synaptic vesicles.⁵⁰
17 Specifically, the ER or Golgi may be highly vulnerable to uncontrolled zinc rises, as
18 we previously reported in *Cln6 nclf* mice.³¹ Moreover, trafficking of multiple metals
19 may be linked at the molecular level. For instance, several zinc transporters were
20 reported to be promiscuous to manganese,⁵¹ and are known to bind copper and/or
21 cobalt, although may not actively transport the latter two metals. It is therefore not
22 surprising that the distributions of these metals throughout NCL model CNS tissue are
23 largely similar. Moreover, studies have also shown a close relationship between the
24 brain homeostasis of copper, zinc and iron.⁵²

25
26 Elevated concentrations of brain metals as observed in *Cln1*, *Cln3* and *Cln5* brains are
27 likely to have pleiotropic consequences in NCL cells. Lipofuscin deposition is
28 enhanced in the presence of iron and copper,⁵³ and lysosomal copper is reported to
29 trigger ROS formation, lysosomal membrane permeabilisation and cell death.⁵⁴ Iron
30 has been reported to induce pro-inflammatory responses in microglia,⁵⁵ and
31 inflammation in turn potentiates cellular iron retention,⁵⁶ thereby creating a feedback
32 loop of metal-deregulation. Moreover, brain iron elevation either in mice fed a high-
33 iron diet, or *Hfe* ko mice with a genetic predisposition to brain iron accumulation
34 results in altered transcription of 5 different NCL-causative genes.^{57, 58} Manganese
35 can enhance inflammatory cytokine production,⁵⁹ and is neurotoxic – overexposure
36 has been linked to parkinsonism (reviewed in ⁶⁰). The dynamic deregulation of cobalt
37 observed here may suggest that directional cobalt transport occurs between different
38 brain regions, or that olfactory neurons, a reported entry route for environmental
39 cobalt,⁶¹ are more susceptible to cobalt overload. Cobalt overload has been reported
40 to induce ROS production in astrocytes and mitochondrial dysfunction in neuronal
41 PC12 cells,^{62,63} common features of NCL diseases. However, deficiency of cobalamin
42 (Vitamin B12), requiring cobalt as a cofactor, has been linked to inflammation and
43 myelin damage (reviewed in ⁶⁴). It is possible that deficiency of cobalt as observed in
44 the hippocampus of 3 month-old *Cln1* ko mice (Fig. 5A) may contribute to the myelin
45 damage reported in these animals.⁶⁵ Therefore impaired biometal homeostasis is
46 capable of initiating and/or exacerbating deregulation of multiple cellular processes
47 that are key pathological features in NCLs, including lipofuscin accumulation,
48 oxidative stress, inflammation, demyelination and deregulation of NCL-causative
49 genes.

1
2
3 1 Copper and zinc both induce robust Mt production through activation of the metal
4 2 responsive transcription factor MTF1,⁶⁶ thus Mt transcript elevation can be used as a
5 3 surrogate marker of metal accumulation. In the present study, we observed significant
6 4 induction of *Mt1* and *Mt2* in *Cln1* ko mouse cortices, as well as an overall trend in
7 5 upregulation of all 3 *Mt* isoforms in *Cln1*, *Cln3* and *Cln5* ko mice. This indicates a
8 6 probable attempt to counteract metal-induced stress via induction of the metal-
9 7 sequestering Mts. However, elevated metals may be restricted to specific subcellular
10 8 pools, as previously described for *Cln6 nclf* mice.³¹ Therefore, increased metal
11 9 content may be sensed as metals transit through the cytoplasm, inducing Mt. The
12 10 altered metal transporter protein expression in some cells may promote metal
13 11 accumulation in specific organelles such as the ER or lysosomes, where cytoplasmic
14 12 Mt may not access aberrantly compartmentalized excess metal pools. Thus Mt may
15 13 not adequately prevent metal-induced toxicity via sequestration of excess
16 14 accumulated metals. Mt induction may also function as a double-edged sword. While
17 15 compensatory upregulation results in a higher metal-buffering capacity, this increased
18 16 capacity for cellular metal retention may increase oxidant-releasable intracellular
19 17 metal stores.⁶⁷ This in turn may be detrimental to cells; zinc liberated from Mt3 upon
20 18 oxidative stress has been linked to neurotoxicity.^{68, 69} Interestingly, we observed a
21 19 dramatic decrease of *Mt2* transcripts in *Cln6 nclf* cerebella (Fig. 6D). To date only a
22 20 single transcriptional repressor of *Mt2* has been reported,⁷⁰ whereas Mts are activated
23 21 by various signals including inflammation, increased metal content, oxidative stress
24 22 and infection and mediate anti-oxidant, neuroregenerative, anti-inflammatory and
25 23 neuroprotective actions in the brain (reviewed in⁶⁶). As demonstrated here for *Cln6*
26 24 *nclf* brains, spatiotemporal *Mt* expression is a dynamic process- significantly
27 25 increased *Mt* expression is indicative of stress responses, whereas reduced *Mt*
28 26 expression is likely to exacerbate neurodegeneration, inflammation and metal
29 27 dyshomeostasis.

30 28
31 29 In this study, we examined the levels of the Zip and ZnT transporters, as these were
32 30 significantly altered in CLN6 disease. No differences were observed in Zip or ZnT
33 31 expression except for a predicted low molecular mass isoform of Zip7 in CLN5 mice.
34 32 However, as the underlying causes of biometal accumulation may be different for
35 33 each NCL variant, cellular expression of copper and iron transporters will be
36 34 investigated in future studies. Moreover, as metal transporters are differentially
37 35 expressed in various CNS cell populations,³¹ and neurodegeneration in NCLs is
38 36 highly regional, changes to metal transporter expression may not be adequately
39 37 detected by bulk analyses. Our previous work indicates that examination of metal
40 38 changes in particular organelles may provide a more accurate picture of subcellular
41 39 metal dyshomeostasis, as altered metal and metal transporter content were detected by
42 40 cellular fractionation and ICP-MS analysis where they were not detectable by bulk
43 41 measurements alone in *Cln6 nclf* mice.³¹ We plan to investigate the metal handling
44 42 dynamics in NCL cells and tissues from other CLN models using a combination of
45 43 techniques capable of measuring metals at subcellular resolution, including
46 44 synchrotron X-ray fluorescence microscopy and fluorescent metal sensors that can be
47 45 targeted to specific organelles.^{48, 71, 72}

48 46
49 47 Both cortical and cerebellar abnormalities have been reported in NCL patients and
50 48 animal models,^{9, 34} and the thalamus is an important pathological region in CLN3
51 49 disease³⁵. A recent study noted the complex progression of atrophy in the brains of
52 50 the *Cln1* and *Cln3* ko mice used in this study.⁷³ Indeed, in *Cln1* ko mice, atrophy in
53 51
54 52
55 53
56 54
57 55
58 56
59 57
60 58

1
2
3 1 certain anteroposterior brain regions was initially apparent at 3 months, stabilized by
4 2 5 months, and neurodegeneration was widespread by 7 months.⁷³ The stabilization
5 3 observed at 5 months of age could represent the temporary efficacy of endogenous
6 4 compensatory mechanisms that ultimately fail due to the presence of persistent
7 5 pathological stressors as the animals succumb to disease by 7 months of age.
8 6 Interestingly, the spatio-temporal patterns of metal accumulation in *Cln1* ko mice
9 7 described here (Fig. 1-5) precede and for the most part predict the previously reported
10 8 progressive regional brain atrophy. The brains of *Cln3* ko mice, however, displayed
11 9 no reduction in brain volume until the age of 21 months, when degeneration was only
12 10 observed in rostrocaudal region 3, which included the hippocampus and
13 11 corticothalamic area,⁷³ although the cerebellum was not analysed in that study.
14 12 Moreover, *Cln3* ko mice were reported to accumulate autofluorescent storage material
15 13 in the retina, but this did not severely affect retinal function as assessed by
16 14 electroretinogram testing in 11 month-old mice.⁷⁴ Similarly, although impaired motor
17 15 function is observed from post-natal day 14 in these mice, rotarod scores did not
18 16 progressively decline with time.⁹ Thus, the subtle changes in metal content in *Cln3* ko
19 17 mice compared to *Cln1* ko, *Cln5* ko and *Cln6 nclf* mice may reflect the mild rate of
20 18 motor and visual symptom progression and late manifestation of brain atrophy in
21 19 these animals. However, it is possible that examination of tissues from older mice
22 20 may have yielded larger changes in metal content.
23 21

24 22 Subtle increases in CNS-wide metal concentrations in *Cln5* ko mice were detected
25 23 from 5 months of age prior to vision loss, although lipofuscin deposition is already
26 24 present. At 5 months, the most prominent increase was observed for cobalt followed
27 25 by copper. By 7 months of age, all CNS regions had significantly elevated metal
28 26 concentrations. It is noteworthy that the regional profile of metal elevation for most
29 27 metals was consistent between 5 month-old *Cln1* ko and 7 month-old *Cln5* ko mice.
30 28

31 29 By contrast, in *Cln6 nclf* mice, tissue metal changes were first apparent in cortex and
32 30 spinal cord, progressing to the cerebellum at a later presymptomatic age. By symptom
33 31 onset at 8 months, biometal changes were evident in cortex and olfactory bulb,
34 32 although the olfactory bulb was the only site of decreased metal content in *Cln6 nclf*
35 33 mice at any age tested. In *Cln6 nclf* mice, the heart was also a site of progressive
36 34 peripheral biometal accumulation, supportive of previously reported cardiac
37 35 dysfunction in NCL patients.⁷⁵ In the models described here, however, the
38 36 abnormalities in metal homeostasis appear to be confined to the CNS, at least at the
39 37 ages tested.
40 38

41 39 The importance of appreciating the benefits and limitations of each NCL disease
42 40 model studied cannot be understated. For example, *Cln3ΔEx1-6* mice used here have
43 41 a mild disease phenotype, but tissue pathology that is reminiscent of JNCL patients,⁸
44 42 while the *Cln3ΔEx7-8* mice display an aggressive form of disease progressing from
45 43 abnormalities during the embryonic stage.⁷ Similarly, *Cln1ΔEx9* mice lack
46 44 progressive visual impairment,⁴ compared to the *Cln1ΔEx4* mice used in this study.³
47 45 *Cln6 nclf* mice carry a naturally occurring mutation in *Cln6*, whereas other NCL
48 46 models are artificially generated. These considerations highlight the utility of
49 47 examining multiple disease models as each may recapitulate particular disease
50 48 features, but will not demonstrate all clinically relevant signs.
51 49

52 50 **CONCLUSION**
53
54
55
56
57
58
59
60

1
2
3
4
5
6
7
8
9
10
11
12
13
14
15
16
17
18
19
20
21
22
23
24
25
26
27
28
29
30
31
32
33
34
35
36
37
38
39
40
41
42
43
44
45
46
47
48
49
50
51
52
53
54
55
56
57
58
59
60

1
2 We have previously demonstrated that deregulation of biometal homeostasis precedes
3 symptoms in 3 natural CLN6 sheep and mouse models, which may be caused by
4 impaired expression of the metal transporter Zip7. In the present study, we extended
5 these findings to include 3 additional models of NCL disease. We observed
6 progressive CNS-localized biometal accumulation, generally prior to symptom onset
7 and relative to the severity of disease in *Cln1*, *Cln3*, and *Cln5* mice, indicating that
8 metal homeostasis defects are a feature of at least 4 genetic forms of NCLs. Increased
9 expression mRNA encoding the metal-responsive anti-oxidant protein, Mt, verified
10 that perturbations to metal homeostasis are present in these models. Given that no
11 significant changes to metal transport proteins were detected, it is currently unclear
12 whether impaired biometal handling is an initiating factor contributing to
13 neurodegeneration, or a consequence of neurodegenerative changes in these mice.
14 Future studies will examine subcellular biometal handling to determine the
15 mechanistic changes underlying biometal accumulation in individual models of NCL
16 disease.

19 EXPERIMENTAL

21 Mice

22 This study used wild type (WT) *Rcc* mice, homozygous transgenic *Cln1* ko
23 (*Cln1ΔEx4³*) and *Cln5* ko mice (*Cln5ΔEx3¹²*), C57BL/6 WT and homozygous *Cln3*
24 ko mice (*Cln3ΔEx1-6⁸*) and WT and *Cln6 nclf* mice.⁷⁶ Animal handling and
25 experimentation were performed in accordance with national and institutional
26 guidelines (National Public Health Institute, University of Helsinki, King's College
27 London and Melbourne University, as well as State Provincial offices of Finland
28 (agreement numbers ESAVI/3474/04.10.03/2012, KEK12-017, and KTL 2005-02;
29 AEC# 1112024). The mice received a standard rodent diet and water, provided *ad*
30 *libitum*. The weights of all *Cln3* and *Cln5* ko mice were typical to that of WT
31 C57BL/6 mice (25-30g for 6-12 months), whereas *Cln1* ko mice progressively lose
32 weight and weigh on average 3-12g less than their WT counterparts. The genotypes of
33 affected *Cln1* ko, *Cln3* ko, *Cln5* ko and *Cln6 nclf* mice were determined as previously
34 described.^{3, 8, 12, 31} Mice were euthanized by an intraperitoneal overdose of 2:1
35 Ketaminol vet (50 mg/ml, Intervet International, Netherlands) and Rompun vet
36 (xylaxin, 20 mg/ml, Bayer Health Care A-G, Germany; for *Cln1* and *Cln5* ko mice) or
37 an intraperitoneal overdose of Lethobarb (for *Cln3* ko mice) and were transcardially
38 perfused with 0.9% (w/v) saline containing 0.01% (w/v) heparin. At post mortem,
39 brains were dissected into the following regions for *Cln1* and *Cln5* ko mice (N=5-8
40 per genotype per age group, for male:female ratios and animal numbers, see
41 supplementary material, Table S1-S2): olfactory bulb, cortex, cerebellum, and brain
42 stem, and immediately frozen in liquid nitrogen. Spinal cords were also collected for
43 analysis. For *Cln3* ko mice (N=5 per genotype per age group), the brains were
44 dissected into: brainstem, cortex, cerebellum and thalamus. The spinal cord, heart and
45 liver were also collected and frozen for metal analyses. For *Cln6 nclf* mice (N=5 per
46 genotype), cortex, cerebellum and spinal cord were collected at post mortem.

48 ICP-MS

1 The metal contents in mouse brain and peripheral tissues were measured using
2 inductively coupled plasma mass-spectrometry (ICP-MS) as previously reported.³²
3 Briefly, each CNS tissue piece from one hemisphere, or half of the peripheral tissue
4 for each mouse was weighed, lyophilized, digested in nitric acid overnight, and heated
5 at 90°C for 20 min. The acid treated samples were then treated with hydrogen
6 peroxide. After 30 min, the samples were heated for a further 15 min at 70°C. All
7 samples were diluted in 1 % nitric acid before being measured using an Agilent 7700
8 series ICPMS instrument using a Helium Reaction Gas Cell. The instrument was
9 calibrated using 0, 5, 10, 50, 100 and 500 ppb of certified multi-element ICPMS
10 standard calibration solutions (Accustandard, New Haven, CT, USA) for a range of
11 elements. 200 ppb of Yttrium (Y89) was used as an internal control (Accustandard).

12 **qRT PCR**

13
14
15 Due to limited amounts of tissue for each mouse cohort, we chose a primary
16 pathogenic tissue for investigation of *Mt* mRNA expression based on previous reports
17 of pathology in these mice, and a secondary tissue with which to perform western
18 blotting analyses. RNA was prepared and DNase treated from 1-5mg of mouse
19 tissues using the MagMax Total RNA isolation kit (Life Technologies, Mulgrave,
20 Victoria, Australia) or Purelink RNA mini kit (Life Technologies). RNA (200ng) was
21 reverse transcribed using the High Capacity cDNA kit (Life Technologies). Mouse
22 endogenous control GAPDH (4352932) and TaqMan gene expression assays for
23 *Mt1A*, *Mt2*, *Mt3* and *Tuba8* were purchased from Life Technologies
24 (Mm00496660_g1, Mm00809556_s1, Mm00496666_g1 and Mm00833707_mH
25 respectively) and qRT-PCR was performed as previously described.³¹ Delta Ct
26 method was used for normalisation of expression relative to β -tubulin or GAPDH.

27 **Western Blotting**

28
29
30 Cell lysates and tissues homogenized with a Dounce tissue grinder were extracted
31 with Phosphosafe (Merck, Kilsyth, Victoria, Australia) containing a protease inhibitor
32 cocktail (Roche, Castle Hill, NSW, Australia) and DNase (Roche). Western blotting
33 was performed as previously described³¹ using antibodies to the following zinc
34 transport proteins: Zip7 (1:2000, Proteintech, Chicago, IL, USA), Zip8 (1:1200,
35 Proteintech), Zip14 (Novus, Littleton, CO, USA), ZnT5 (1:1000, Abcam, Cambridge,
36 UK), ZnT6 (1:1200, Proteintech), ZnT7 (1:1000, Proteintech). Where visibly different
37 between control and transgenic animals ($N \geq 5$ animals per genotype), target band
38 intensities were compared to control bands (ImageJ, Bethesda, MD, USA) on blots
39 probed with antibodies against β -tubulin or total ERK used as controls to normalize
40 protein concentrations in affected and control animals.

41 **Statistical Analysis**

42
43 The effects of genotype and brain region on metal concentrations were examined
44 using 2-way ANOVA in GraphPad Prism software (GraphPad Software, La Jolla, CA,
45 USA). If either statistically significant main effects or interactions of brain region and
46 genotype were detected, the regions with differing metal concentrations were
47 individually determined using Bonferonni posttests. 1-way ANOVA was used to test
48 the effect of genotype on *Mt* mRNA levels.

49 **ABBREVIATIONS**

1			
2			
3	1	CNS	central nervous system
4	2	INCL	Infantile NCL
5	3	JNCL	Juvenile NCL
6	4	ko	knockout
7	5	LSD	lysosomal storage disorder
8	6	Mt	metallothionein
9	7	NCL	Neuronal Ceroid Lipofuscinosis
10	8	vLINCL	variant late infantile NCL
11			
12	9		

13 ACKNOWLEDGEMENTS

14 This work was supported by The Sigrid Juselius Foundation [grant number 1512032
15 to K.M.K]; the Academy of Finland [grant number 135625 to K.M.K]; the Finnish
16 Cultural Foundation [grant to K.M.K]; the Australian Research Council (ARC)
17 [DP110101368]; and National Health and Medical Research Council of Australia
18 (NHMRC) [628946]. A.R.W. is a recipient of an ARC Future Fellowship
19 [FT100100674]. Essi Kaiharju is thanked for the excellent technical assistance with
20 mouse experiments. The funding sources had no influence in study design; in the
21 collection, analysis and interpretation of data; in the writing of the report; and in the
22 decision to submit the article for publication. AG, KMK, ARW designed experiments.
23 AG, EP, CD, AC, TB, IV, AW, AJ, JC performed experiments. AG, EP, KMK, IV
24 analysed the data. AG and KMK wrote the manuscript. PJC, JK, AJ, JC, ARW,
25 provided reagents. KMK, ARW, PJC, JK, TB, AW provided critical revisions of the
26 manuscript.
27
28

29
30 24
31
32
33
34
35
36
37
38
39
40
41
42
43
44
45
46
47
48
49
50
51
52
53
54
55
56
57
58
59
60

FIGURE LEGENDS

Fig. 1. Zinc concentrations in the brain of *Cln1*, *Cln3* and *Cln5* ko mice. Zinc concentrations in CNS of (A) 3 month-old, (B) 4 month-old, (C) 5 month-old or (D) 7 month-old WT mice, *Cln1* and *Cln5* ko mice were measured using ICP-MS. Zinc concentrations in CNS of (E) 6 month-old and (F) 12 month-old WT mice and *Cln3* ko mice were measured using ICP-MS. The concentrations of zinc in each tissue are expressed as mean \pm S.D. Values correspond to μg metal/g tissue. * $p < 0.05$, ** $p < 0.01$, *** $p < 0.001$ by 2-way ANOVA and Bonferroni posttests. HC, hippocampus; CX, cortex; CB, cerebellum; OB, olfactory bulb; SC, spinal cord; BS, brainstem; TH, thalamus.

Fig. 2. Copper concentrations in the brain of *Cln1*, *Cln3* and *Cln5* ko mice. Copper concentrations in CNS of (A) 3 month-old, (B) 4 month-old, (C) 5 month-old or (D) 7 month-old WT mice, *Cln1* and *Cln5* ko mice were measured using ICP-MS. Copper concentrations in CNS of (E) 6 month-old and (F) 12 month-old WT mice and *Cln3* ko mice were measured using ICP-MS. The concentrations of copper in each tissue are expressed as mean \pm S.D. Values correspond to μg metal/g tissue. * $p < 0.05$, ** $p < 0.01$, *** $p < 0.001$ by 2-way ANOVA and Bonferroni posttests. Statistically significant main effects of copper in WT compared with CLN3 brains were calculated by 2-way ANOVA. HC, hippocampus; CX, cortex; CB, cerebellum; OB, olfactory bulb; SC, spinal cord; BS, brainstem; TH, thalamus.

Fig. 3. Manganese concentrations in the brain of *Cln1*, *Cln3* and *Cln5* ko mice. Manganese concentrations in CNS of (A) 3 month-old, (B) 4 month-old, (C) 5 month-old or (D) 7 month-old WT mice, *Cln1* and *Cln5* ko mice were measured using ICP-MS. Manganese concentrations in CNS of (E) 6 month-old and (F) 12 month-old WT mice and *Cln3* ko mice were measured using ICP-MS. The concentrations of manganese in each tissue are expressed as mean \pm S.D. Values correspond to μg metal/g tissue. * $p < 0.05$, ** $p < 0.01$, *** $p < 0.001$ by 2-way ANOVA and Bonferroni posttests. HC, hippocampus; CX, cortex; CB, cerebellum; OB, olfactory bulb; SC, spinal cord; BS, brainstem; TH, thalamus.

Fig. 4. Iron concentrations in the brain of *Cln1*, *Cln3* and *Cln5* ko mice. Iron concentrations in CNS of (A) 3 month-old, (B) 4 month-old, (C) 5 month-old or (D) 7 month-old WT mice, *Cln1* and *Cln5* ko mice were measured using ICP-MS. Iron concentrations in CNS of (E) 6 month-old and (F) 12 month-old WT mice and *Cln3* ko mice were measured using ICP-MS. The concentrations of iron in each tissue are expressed as mean \pm S.D. Values correspond to μg metal/g tissue. * $p < 0.05$, ** $p < 0.01$, *** $p < 0.001$ by 2-way ANOVA and Bonferroni posttests. Statistically significant main effects of iron in WT compared with CLN3 brains were calculated by 2-way ANOVA. HC, hippocampus; CX, cortex; CB, cerebellum; OB, olfactory bulb; SC, spinal cord; BS, brainstem; TH, thalamus.

Fig. 5. Cobalt concentrations in the brain of *Cln1*, *Cln3* and *Cln5* ko mice. Cobalt concentrations in CNS of (A) 3 month-old, (B) 4 month-old, (C) 5 month-old or (D) 7 month-old WT mice, *Cln1* and *Cln5* ko mice were measured using ICP-MS. Cobalt concentrations in CNS of (E) 6 month-old and (F) 12 month-old WT mice and *Cln3* ko mice were measured using ICP-MS. Cobalt levels were below detection limits in the thalamus of WT and *Cln3* ko mice. The concentrations of cobalt in each tissue are

expressed as mean \pm S.D. Values correspond to μg metal/g tissue. * $p < 0.05$, ** $p < 0.01$, *** $p < 0.001$ by 2-way ANOVA and Bonferroni posttests. Statistically significant main effects of cobalt in WT compared with CLN3 brains were calculated by 2-way ANOVA. HC, hippocampus; CX, cortex; CB, cerebellum; OB, olfactory bulb; SC, spinal cord; BS, brainstem; TH, thalamus.

Fig. 6. Metallothionein mRNA induction in NCL mutant mice. Metallothionein (*Mt1*, 2 or 3) mRNA expression in was measured using qRT-PCR in (A) the cortex of 5 month-old WT, *Cln1* and *Cln5* ko mice, (B) the cerebellum of 6 month-old WT or *Cln3* ko mice, and (C-E) the cerebellum, cortex and spinal cords of 3 month-old *Cln6 nclf* mice. Expression values were normalized to tubulin or GAPDH using the delta Ct method. Data are expressed as fold Mt mRNA compared to WT controls. * $p < 0.05$, ** $p < 0.01$, *** $p < 0.001$ by 1-way or 2-way ANOVA and Bonferroni posttests, as appropriate.

Fig. 7. Biometal trafficking pathways in the brains of *Cln1*, *Cln3* and *Cln5* ko mice. Representative immunoblots of homogenates (5-40 μg) isolated from the cerebellum of 7 month-old WT and *Cln5* ko mice, 5 month-old WT and *Cln1* ko mice or the cortex of 6 month-old WT and *Cln3* ko mice (minimum N=5 animals per group) probed with antibodies directed against a range of metal transporter proteins of the Zip and ZnT families. β -tubulin was used as loading controls for *Cln1* and *Cln5* ko mice, whereas total ERK was used as a control for *Cln3* ko mice. N.D. no protein detected.

TABLES

Table 1. Characteristics of mouse models analysed.

^ motor dysfunction in not progressive

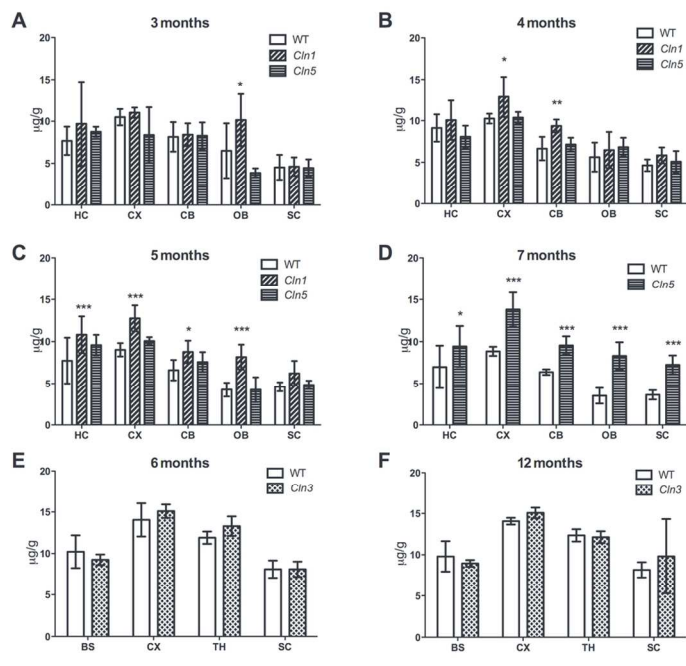
* HC, hippocampus; CX, cortex; CB, cerebellum; OB, olfactory bulb; SC, spinal cord; BS, brainstem; TH, thalamus.

Disease	Model	Visual/motor symptoms	Storage material	Lifespan	Ages analysed	Tissues analysed*
INCL	<i>Cln1</i> Δ <i>Ex4</i> ³	3.5/4m ³	3m ³	6.5m ³	3,4,5m	HC, CX, CB, OB, SC
vLINCL	<i>Cln5</i> Δ <i>Ex3</i> ¹²	5.2m/>8m ¹²	3m ¹²	>8m ³⁴	3,4,5,7m	HC, CX, CB, OB, SC
vLINCL	<i>Cln6 nclf</i> ⁷⁶	4/8m ⁷⁶	P11 ⁷⁶	12m ⁷⁶	3m	CX, CB, SC
JNCL	<i>Cln3</i> Δ <i>Ex1-6</i> ⁸	>11m ⁷⁴ /E14 ⁹ⁿ	5m ⁸	>21m ⁷³	6,12m	BS, CX, TH, SC, CB

1
2
3
4
5
6
7
8
9
10
11
12
13
14
15
16
17
18
19
20
21
22
23
24
25
26
27
28
29
30
31
32
33
34
35
36
37
38
39
40
41
42
43
44
45
46
47
48
49
50
51
52
53
54
55
56
57
58
59
60
1 REFERENCES

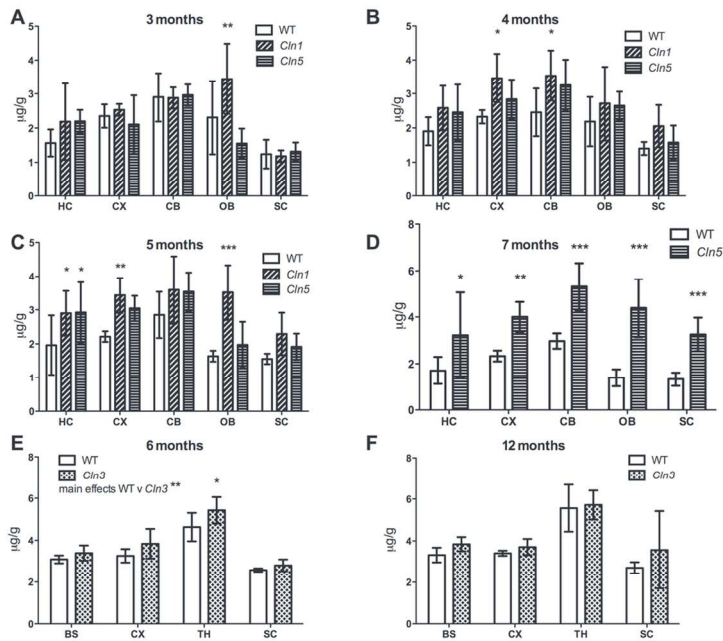
1. R.M. Boustany, *Nat Rev Neurol*, 2013.
2. J. Vesa, E. Hellsten, et al., *Nature*, 1995, **376**, 584-587.
3. A. Jalanko, J. Vesa, et al., *Neurobiol Dis*, 2005, **18**, 226-241.
4. P. Gupta, A.A. Soyombo, et al., *Proc Natl Acad Sci U S A*, 2001, **98**, 13566-13571.
5. C.C. Pontikis, S.L. Cotman, et al., *Neurobiol Dis*, 2005, **20**, 823-836.
6. A. Getty, A.D. Kovacs, et al., *PLoS One*, 2013, **8**, e66203.
7. S.L. Cotman, V. Vrbanac, et al., *Hum Mol Genet*, 2002, **11**, 2709-2721.
8. H.M. Mitchison, D.J. Bernard, et al., *Neurobiol Dis*, 1999, **6**, 321-334.
9. J.M. Weimer, J.W. Benedict, et al., *Brain Res*, 2009, **1266**, 93-107.
10. V. Holmberg, A. Jalanko, et al., *Neurobiol Dis*, 2004, **16**, 29-40.
11. S.E. Haddad, M. Khoury, et al., *Electrophoresis*, 2012, **33**, 3798-3809.
12. O. Kopra, J. Vesa, et al., *Hum Mol Genet*, 2004, **13**, 2893-2906.
13. A. Jalanko and T. Braulke, *Biochim Biophys Acta*, 2009, **1793**, 697-709.
14. K. Kollmann, K. Uusi-Rauva, et al., *Biochim Biophys Acta*, 2013, **1832**, 1866-1881.
15. M.J. Oswald, D.N. Palmer, et al., *Neurobiol Dis*, 2005, **20**, 49-63.
16. A. Lyly, S.K. Marjavaara, et al., *Hum Mol Genet*, 2008, **17**, 1406-1417.
17. L. Ahtiainen, J. Kolikova, et al., *Neurobiol Dis*, 2007, **28**, 52-64.
18. M.L. Schmiedt, T. Blom, et al., *Neurobiol Dis*, 2012, **46**, 19-29.
19. S. Jabs, A. Quitsch, et al., *J Neurochem*, 2008, **106**, 1415-1425.
20. D. Rakheja, S.B. Narayan, et al., *Biochem Biophys Res Commun*, 2004, **317**, 988-991.
21. R. Goswami, M. Ahmed, et al., *J Neurosci Res*, 2005, **81**, 208-217.
22. A. Lyly, C. von Schantz, et al., *BMC Cell Biol*, 2009, **10**, 83.
23. A. Sharifi, M. Kousi, et al., *Hum Mol Genet*, 2010, **19**, 4497-4514.
24. S. Bolognin, L. Messori, et al., *Neuromolecular Med*, 2009, **11**, 223-238.
25. C. Andreini, L. Banci, et al., *J Proteome Res*, 2006, **5**, 196-201.
26. A.I. Bush and C.C. Curtain, *Eur Biophys J*, 2008, **37**, 241-245.
27. P.J. Crouch, L.W. Hung, et al., *Proc Natl Acad Sci U S A*, 2009, **106**, 381-386.
28. N.G. Faux, C.W. Ritchie, et al., *J Alzheimers Dis*, 2010, **20**, 509-516.
29. L.W. Hung, V.L. Villemagne, et al., *J Exp Med*, 2012, **209**, 837-854.
30. C.P. Soon, P.S. Donnelly, et al., *J Biol Chem*, 2011, **286**, 44035-44044.
31. K.M. Kanninen, A. Grubman, et al., *Biol Open*, 2013, **2**, 635-646.
32. K.M. Kanninen, A. Grubman, et al., *PLoS One*, 2013, **8**, e58644.
33. C. von Schantz, J. Saharinen, et al., *BMC Genomics*, 2008, **9**, 146.
34. C. von Schantz, C. Kielar, et al., *Neurobiol Dis*, 2009, **34**, 308-319.
35. T. Autti, R. Raininko, et al., *Neuroradiology*, 1996, **38**, 476-482.
36. A. Krezel and W. Maret, *J Am Chem Soc*, 2007, **129**, 10911-10921.
37. I. Sekler, S.L. Sensi, et al., *Mol Med*, 2007, **13**, 337-343.
38. A.M. Das, R. von Harlem, et al., *Eur J Paediatr Neurol*, 2001, **5 Suppl A**, 143-146.
39. K. Luiro, O. Kopra, et al., *J Neurosci Res*, 2006, **84**, 1124-1138.
40. Y. Cao, J.F. Staropoli, et al., *PLoS One*, 2011, **6**, e17118.
41. J. Bras, A. Verloes, et al., *Hum Mol Genet*, 2012, **21**, 2646-2650.
42. F.H. Farias, R. Zeng, et al., *Neurobiol Dis*, 2011, **42**, 468-474.

- 1
2
3 1 43. A. Wohlke, U. Philipp, et al., *PLoS Genet*, 2011, **7**, e1002304.
4 2 44. J.F. Staropoli, A. Karaa, et al., *Am J Hum Genet*, 2012, **91**, 202-208.
5 3 45. J.J. Hwang, S.J. Lee, et al., *J Neurosci*, 2008, **28**, 3114-3122.
6 4 46. S.L. Sensi, H.Z. Yin, et al., *Proc Natl Acad Sci U S A*, 1999, **96**, 2414-2419.
7 5 47. P.A. Adlard, J.M. Parncutt, et al., *J Neurosci*, 2010, **30**, 1631-1636.
8 6 48. Y. Qin, P.J. Dittmer, et al., *Proc Natl Acad Sci U S A*, 2011, **108**, 7351-7356.
9 7 49. W. Maret and A. Krezel, *Mol Med*, 2007, **13**, 371-375.
10 8 50. C.J. Frederickson, L.J. Giblin, 3rd, et al., *J Neurosci Methods*, 2006, **154**, 19-
11 9 29.
12 10 51. K. Girijashanker, L. He, et al., *Mol Pharmacol*, 2008, **73**, 1413-1423.
13 11 52. S. Bolognin, F. Pasqualetto, et al., *PLoS One*, 2012, **7**, e47063.
14 12 53. A. Hohn, T. Jung, et al., *Free Radic Biol Med*, 2010, **48**, 1100-1108.
15 13 54. J. Pourahmad, S. Ross, et al., *Free Radic Biol Med*, 2001, **30**, 89-97.
16 14 55. V. Mehta, W. Pei, et al., *PLoS One*, 2013, **8**, e57573.
17 15 56. P. Urrutia, P. Aguirre, et al., *J Neurochem*, 2013, **126**, 541-549.
18 16 57. D. Johnstone, R.M. Graham, et al., *Brain Res*, 2012, **1448**, 144-152.
19 17 58. D. Johnstone and E.A. Milward, *Neurochem Int*, 2010, **56**, 856-863.
20 18 59. N.M. Filipov, R.F. Seegal, et al., *Toxicol Sci*, 2005, **84**, 139-148.
21 19 60. T.R. Guilarte, *Front Aging Neurosci*, 2013, **5**, 23.
22 20 61. E. Persson, J. Henriksson, et al., *Toxicol Lett*, 2003, **145**, 19-27.
23 21 62. G. Wang, T.K. Hazra, et al., *Nucleic Acids Res*, 2000, **28**, 2135-2140.
24 22 63. O. Karovic, I. Tonazzini, et al., *Biochem Pharmacol*, 2007, **73**, 694-708.
25 23 64. G. Scalabrino, *Prog Neurobiol*, 2009, **88**, 203-220.
26 24 65. T. Blom, M.L. Schmiedt, et al., *Dis Model Mech*, 2013, **6**, 342-357.
27 25 66. M.O. Pedersen, R. Jensen, et al., *Biofactors*, 2009, **35**, 315-325.
28 26 67. A. Krezel and W. Maret, *Biochem J*, 2007, **402**, 551-558.
29 27 68. K.D. Kroncke, K. Fehsel, et al., *Biochem Biophys Res Commun*, 1994, **200**,
30 28 1105-1110.
31 29 69. J.Y. Lee, J.H. Kim, et al., *Exp Neurol*, 2003, **184**, 337-347.
32 30 70. C.M. Tang, J. Westling, et al., *Mol Cell Biol*, 1999, **19**, 680-689.
33 31 71. C.P. Montgomery, B.S. Murray, et al., *Acc Chem Res*, 2009, **42**, 925-937.
34 32 72. K.A. Price, P.J. Crouch, et al., *Metallomics*, 2011, **3**, 1280-1290.
35 33 73. T.G. Kuhl, S. Dihanich, et al., *J Child Neurol*, 2013, **28**, 1117-1122.
36 34 74. G.M. Seigel, A. Lotery, et al., *Mol Cell Neurosci*, 2002, **19**, 515-527.
37 35 75. P. Michielsen, J.J. Martin, et al., *Eur Neurol*, 1984, **23**, 166-172.
38 36 76. R.T. Bronson, L.R. Donahue, et al., *Am J Med Genet*, 1998, **77**, 289-297.
39
40
41
42
43
44
45
46
47
48
49
50
51
52
53
54
55
56
57
58
59
60



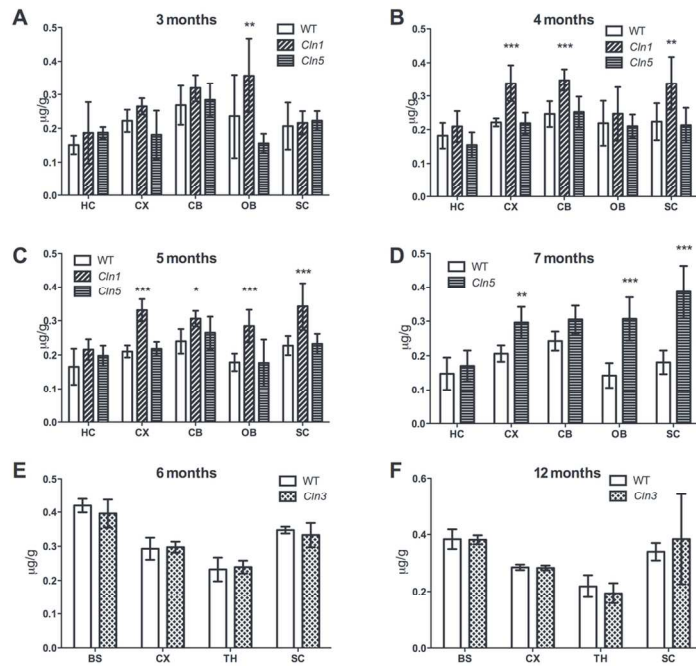
119x83mm (300 x 300 DPI)

1
2
3
4
5
6
7
8
9
10
11
12
13
14
15
16
17
18
19
20
21
22
23
24
25
26
27
28
29
30
31
32
33
34
35
36
37
38
39
40
41
42
43
44
45
46
47
48
49
50
51
52
53
54
55
56
57
58
59
60



117x80mm (300 x 300 DPI)

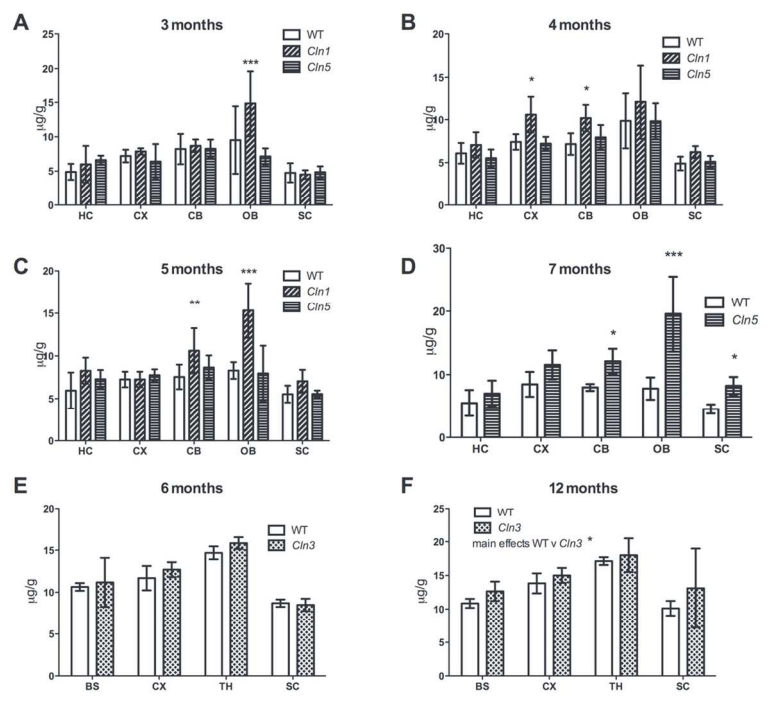
1
2
3
4
5
6
7
8
9
10
11
12
13
14
15
16
17
18
19
20
21
22
23
24
25
26
27
28
29
30
31
32
33
34
35
36
37
38
39
40
41
42
43
44
45
46
47
48
49
50
51
52
53
54
55
56
57
58
59
60



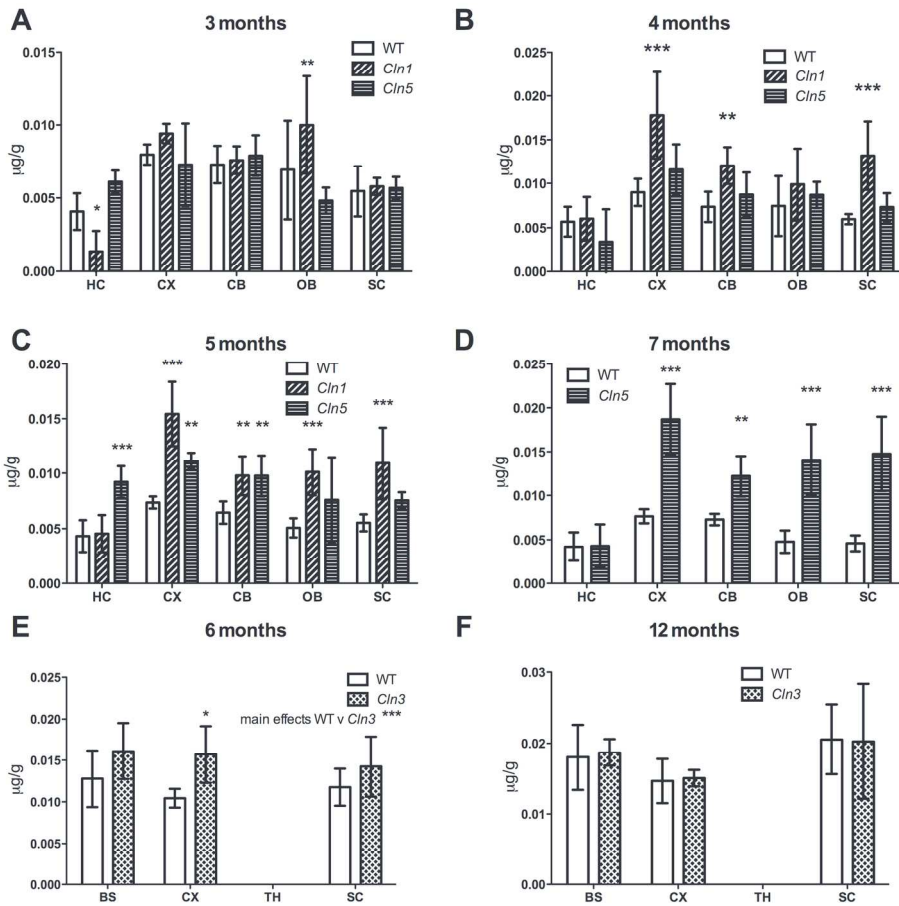
122x87mm (300 x 300 DPI)

1
2
3
4
5
6
7
8
9
10
11
12
13
14
15
16
17
18
19
20
21
22
23
24
25
26
27
28
29
30
31
32
33
34
35
36
37
38
39
40
41
42
43
44
45
46
47
48
49
50
51
52
53
54
55
56
57
58
59
60

1
2
3
4
5
6
7
8
9
10
11
12
13
14
15
16
17
18
19
20
21
22
23
24
25
26
27
28
29
30
31
32
33
34
35
36
37
38
39
40
41
42
43
44
45
46
47
48
49
50
51
52
53
54
55
56
57
58
59
60

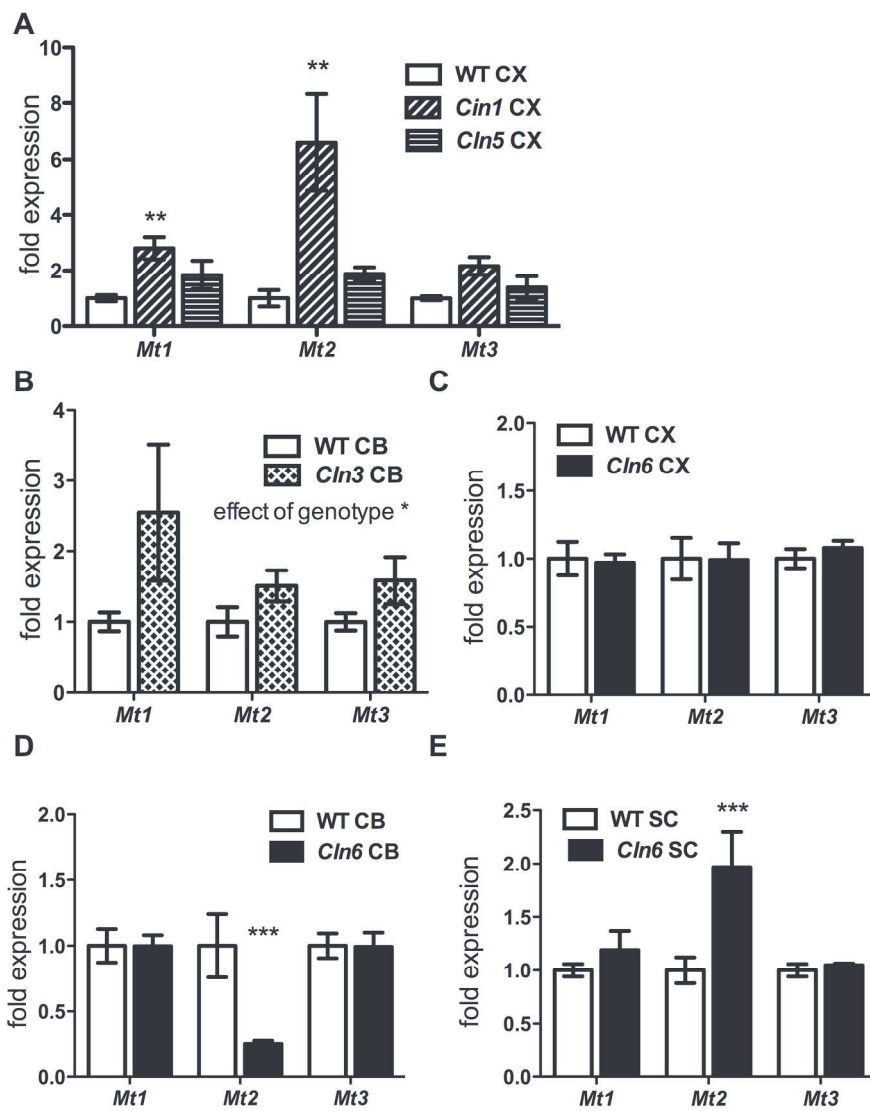


126x93mm (300 x 300 DPI)



167x163mm (300 x 300 DPI)

1
2
3
4
5
6
7
8
9
10
11
12
13
14
15
16
17
18
19
20
21
22
23
24
25
26
27
28
29
30
31
32
33
34
35
36
37
38
39
40
41
42
43
44
45
46
47
48
49
50
51
52
53
54
55
56
57
58
59
60



203x241mm (300 x 300 DPI)

